Journal of Structural Geology 188 (2024) 105265

Contents lists available at ScienceDirect

Journal of Structural Geology

journal homepage: www.elsevier.com/locate/jsg

Normal fault architecture, evolution, and deformation mechanisms in basalts, Húsavik, Iceland: Impact on fluid flow in geothermal reservoirs and seismicity

Luca Smeraglia [a,b,*], Andrea Billi [a], Eugenio Carminati [c], Luca Aldega [c], Alasdair Skelton [d], Gabrielle Stockmann [e], Erik Sturkell [f]

[a] Consiglio Nazionale delle Ricerche, IGAG, Rome, Italy
[b] Chrono-Environnement, Université de Bourgogne Franche-Comté, 16 Route de Gray, 25000, Besançon, France
[c] Dipartimento di Scienze della Terra, Sapienza University of Rome, Italy
[d] Department of Geological Sciences, Stockholm University, 106 91, Stockholm, Sweden
[e] Jarvik GeoConsulting AB, 413 21, Gothenburg, Sweden
[f] Department of Earth Sciences, University of Gothenburg, 413 90, Gothenburg, Sweden

ARTICLE INFO

Keywords:
Geothermal energy
Fractured reservoir
Faults in basalt
Fluid flow
Fault permeability

ABSTRACT

Faults within layered basaltic sequences significantly influence hydrothermal fluid flow in shallow geothermal reservoirs and potentially during CO_2 sequestration and storage. Nevertheless, their characterization regarding fault zone architecture, fluid flow, deformation mechanisms, and seismic potential remains underdeveloped. This study addresses this gap by integrating structural and microstructural observations with X-ray diffraction analyses of exposed normal-transtensional faults associated with the seismically active Húsavík-Flatey Fault in the Tjörnes Fracture Zone, Northern Iceland. Our findings demonstrate that the evolution of basalt-hosted normal-transtensional faults progresses through distinct stages: (1) low-displacement fault propagation from pre-existing cooling joints; (2) fault linkage via dilational jogs; (3) damage zone/fault core growth through brecciation and cataclastic processes; (4) shear localization along sharp slip surfaces; and (5) smearing of volcaniclastic interbeds along the principal fault plane. Evidence of shear localization, truncated clasts, and hydrothermal breccias/veins suggests repeated seismic slip events facilitated by overpressured fluids. Conversely, the presence of clay-rich foliated cataclasite indicates aseismic slips during interseismic periods. Slip along fault jogs, bends, geometric irregularities, and orientation changes causes the dilatant opening of the fault planes and extensional horsetail fractures at fault tips. These structures create main tabular zones for lateral movement of hydrothermal fluids parallel to the fault strike in shallow geothermal reservoirs situated in active extensional-transtensional tectonic settings. In addition, the dilational jogs and the intersection of horsetail veins with the hosting faults may define linear zones of high structural permeability and intense localized fluid flow parallel to the σ2 paleostress orientation and finally mineral precipitation. The results of this study can be utilized to improve models of geothermal fluid flow for enhanced recovery in basaltic reservoirs and assess seismic risk in basaltic faults.

1. Introduction

Layered basaltic sequences have recently garnered significant interest due to their potential as reservoirs for both conventional and enhanced geothermal fluids (Arnorsson, 1995) and for CO_2 sequestration and storage, exemplified by the Carbfix CO_2-injection facilities in Iceland (Oelkers and Gislason, 2023). In geothermal exploration and resource development, understanding the structural architecture and permeability of basalt-hosted faults is crucial, as these faults strongly control fluid pathways and recharge areas in geothermal systems (Liotta et al., 2020, 2021). Additionally, comprehending the deformation mechanisms, frictional behavior, and sealing potential of basalt-hosted faults is essential to predict the potential for induced earthquakes during subsurface CO_2 injection (White and Foxall, 2016) or fluid injection operations associated with geothermal energy exploitation (Llenos et al., 2013).

* Corresponding author. Consiglio Nazionale delle Ricerche, IGAG, Rome, Italy.
E-mail address: luca.smeraglia@cnr.it (L. Smeraglia).

https://doi.org/10.1016/j.jsg.2024.105265
Received 2 April 2024; Received in revised form 20 September 2024; Accepted 22 September 2024
Available online 24 September 2024

Significant progress has been made in characterizing faults and fault-rock assemblages in carbonate rocks (Delle Piane et al., 2017) and layered clastic sequences (Vrolijk et al., 2016). However, the evolution, structures, and microstructures of basalt-hosted faults, as well as their frictional and permeability behavior, are still poorly understood. Current knowledge primarily focuses on the general characteristics, mechanics, growth mechanisms, and interactions of near-surface (<500 m depths) faults in basalts (Gudmundsson, 1992; Acocella et al., 2003; Grant and Kattenhorn, 2004; Martel and Langley, 2006), particularly for dilatant faults (Holland et al., 2006; Tibaldi et al., 2016a,b, 2020; Bubeck et al., 2018; Kettermann et al., 2019; von Hagke et al., 2019; Weismüller et al., 2019). However, only a few studies have addressed the evolution, architecture, microstructure, hydraulic properties, and fault-fluid interactions of fault zones formed at greater depths in layered basaltic sequences (Walker et al., 2011, 2012, 2013a, 2013b; Liotta et al., 2020, 2021; Bamberg et al., 2022, 2023). In addition, laboratory studies on the frictional behavior and microstructures of basaltic gouges are limited (Zhang et al., 2017; Giacomel et al., 2018, 2021; Ikari et al.,

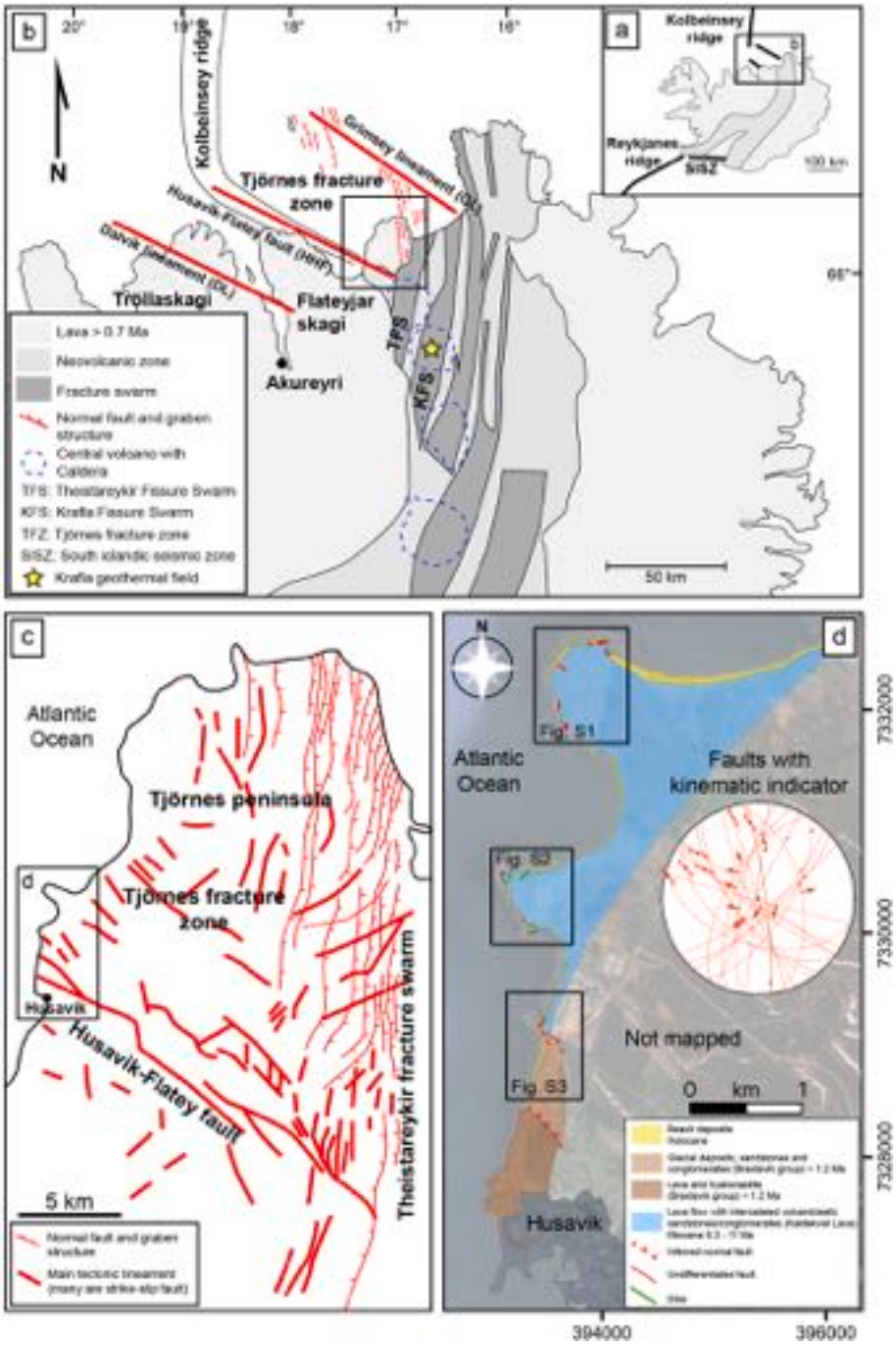

Fig. 1. **(a)** Simplified tectonic sketch of Iceland and adjoining oceans. The darker grey area refers to the onshore location of the axial rift zone. Modified after Gudmundsson (1995). **(b)** Simplified geological map of northern Iceland. Faults are indicated only for the area between the Grimsey and Húsavik-Flatey faults. The solid rectangle shows the location of the map in Fig. 2. Modified after Gudmundsson (1995). **(c)** Tectonic map of the Tjörnes Peninsula and adjoining area, showing major faults. The solid rectangle shows the location of the map of panel (d). Modified after Gudmundsson et al. (1993). **(d)** Geological map of the Húsavik area and of Flateyjarskagi peninsula with a stereoplot including measured faults with kinematic indicators. Faded in the background, satellite photo from Google Earth. The solid rectangles show the location of the maps in Figs. S1, S2 and S3 (Supplemental material).

2020; Zhong et al., 2023) and often lack validation through comparison with natural examples.

This study aims to bridge this gap by providing a detailed description of fault zone structures, deformation mechanisms, and fault-fluid interactions in natural fault zones exhumed from ~1.5 km depth (Sæmundsson and Karson, 2006). These fault zones, formed in an interlayered basaltic-volcaniclastic sequence intersected by dikes, are located within the seismically active (up to M6 earthquakes) Húsavik--Flatey fault zone in Northern Iceland (Fig. 1), part of a transform fault system (Gudmundsson, 1993).

The main objective of this research is to propose a conceptual model for the development of normal-transtensional faults and fault-fluid interactions in interlayered basaltic-volcaniclastic sequences, with implications for structurally controlled hydrothermal fluid flow in basalt-hosted geothermal reservoirs and the seismic cycle. By combining field structural analyses with microstructural observations, we studied several exhumed faults with displacements ranging from <1 m to a few tens of meters and associated fault-controlled mineralizations, describing fault structures from the field to the micro-scale. We also compared natural microstructures with those developed during shear experiments on basaltic gouges. Our results are compared with other studies of basalt-hosted fault structures exhumed from depths >500 m in the Faroe Islands (Walker et al., 2012, 2013a, 2013b; Bamberg et al., 2022, 2023) and Iceland (Liotta et al., 2020, 2021).

Given the increasing economic significance of subsurface reservoirs in basalts, the results of this study are potentially of broad interest to scientists working on geothermal exploration and exploitation, as well as CO_2 capture and storage, with implications for reservoir static and dynamic modeling. Moreover, the Húsavik-Flatey Fault has been a site for monitoring earthquake hydrogeochemical precursors for nearly two decades (Skelton et al., 2019). This fault experienced a major earthquake in 1872, and a steady stress build-up since then is predicted to be released by a future large earthquake (up to M6.8, according to Metzger et al., 2013). Therefore, a better understanding of the structural architecture of this fault and fault-fluid interactions can provide new insights into fault-related fluid circulation in seismically active faults and enhance the surveillance and identification of potential earthquake precursors.

2. Geological setting

Iceland is situated on the North Atlantic mid-ocean ridge, with exposed rocks primarily comprising layered oceanic crust basalts, interlayered basaltic-volcaniclastic sequences, and pyroclastic rocks (Sæmundsson, 1979). Specifically, Iceland lies at the intersection of the Reykjanes Ridge to the south and the Kolbeinsey Ridge to the north (Fig. 1a; Garcia et al., 2003). These ridges are offset by 100 km, a displacement accommodated by the Tjörnes Fracture Zone (TFZ) in the north and the South Iceland Seismic Zone (SISZ) in the south, which are the sites of Iceland's largest earthquakes.

The TFZ is a seismically active, complex fracture and fault zone extending 120 km east-west and 50 km north-south, characterized by normal faults and grabens (Homberg et al., 2010; Rögnvaldsson et al., 1998; Eiríksson et al., 2021; Tibaldi et al., 2016a, 2016b, 2020). It comprises three tectonic zones: the Grímsey Lineament (GL), the Húsavík-Flatey Fault (HFF), and the Dalvík Lineament (DL).

Stefánsson et al. (2008) documented the earthquake activity in the TFZ, listing all M > 6 earthquakes from 1755 to 2007, with ten such events occurring in that period and one M 6 earthquake in 2020. In the GL and DL, most earthquakes align more north-south compared to the HFF. These alignments and the related focal mechanisms indicate sinistral strike-slip motion along north-south faults, whereas the HFF, striking SSE-NNW, exhibits dextral transtensional kinematics and acts as a transform fault, almost parallel to the plate spreading vector.

The plate boundary is divided into two arms, the HFF and GL, with the Tjörnes Peninsula lying between them. Using GPS data, Metzger et al. (2013) estimated that about 40% of the spreading occurs along the HFF boundary, and 60% along the GL. Several volcano systems along the GL, arranged en echelon, connect the northern volcanic zone to the Kolbeinsey Ridge. The onshore segment of the HFF has been locked since the start of the Krafla rifting episode (1975–84) (Björnsson, 1985), with no observed earthquakes since, although strain is continuously increasing (Metzger et al., 2013). The HFF terminates to the east at the north-south trending Theistareykjabunga volcanic system. North-south trending faults offset the 9800 B P Stóravítishraun lava, which is a lava shield within the Theistareykjabunga volcano (Hjartarson, 2011). An M 6 earthquake in 2002 at the junction of the Kolbeinsey Ridge and GL, near the study area of this paper, has been studied and monitored to understand earthquake hydrogeochemical precursors in groundwater. In fact, the area has hosted a groundwater monitoring station for more than twenty years for the identification of potential hydrogeochemical precursors of earthquakes (Claesson et al., 2004; Skelton et al., 2016; 2019; Barbieri et al., 2021; Boschetti et al., 2022).

The HFF displays dextral transtensional kinematics (Angelier et al., 2000; Bergerat et al., 2000) with pull-apart basins at right-stepping overlap zones and push ridges at left-stepping overlap zones (Gudmundsson, 1993; Tibaldi et al., 2016a, 2016b, 2020). In some areas, sinistral strike-slip kinematics have been observed at the SE tip of the Húsavík-Flatey Fault (Liotta et al., 2021). The fault has accommodated several kilometers, potentially tens of kilometers, of horizontal displacement (Sæmundsson, 1974) and several hundred meters, possibly more than a thousand meters, of vertical displacement (Gudmundsson, 1993).

Exposures of the HFF are located in the southern part of the Tjörnes Peninsula, near the town of Húsavík (Fig. 1a and b). In this region and in the nearby Flateyjarskagi Peninsula (Fig. 1), subsidiary faults and fault zones exhibit extensional to dextral strike-slip kinematics, consistent with the regional dextral movement along the HFF (Bergerat et al., 2000). These fault zones feature mineralized veins (Gudmundsson, 1999; Hummel et al., 2022; Wästeby et al., 2014). Mineralizations and rock alterations associated with the Húsavík-Flatey Fault have been interpreted as resulting from fluids injected into the fault during earthquakes (Andrén et al., 2016). Near Húsavík, faults displace Miocene (5.3–11 Ma) Kaldakvisl lava flows intercalated with volcaniclastic deposits, and lava/hyaloclastite and glacial deposits, sandstones, and conglomerates of the Breidavik Group (<1.2 Ma) (Eiríksson et al., 2021).

3. Methods

To characterize the fault zone structures, we conducted geological-structural mapping at a 1:10,000 scale along the coastal cliffs northeast of Húsavik (Fig. 2b and Figs. S1, S2, and S3). We studied in detail fault zones exposed in ten localities and three dikes (Table S1). Most of the faults exhibit displacements of less than 10 m. However, at Hédinshöfdi, we examined a fault with displacements of several tens of meters. Field data collection included measurements of bedding, fracture/vein, dike, and fault attitudes, as well as kinematic indicators such as slickenfibers and slickenlines. These data were gathered using an iPhone 12 Pro equipped with FieldMove Clino software (by Petroleum Expert), with daily accuracy checks using a Brunton analog compass.

For microstructural and deformation mechanism characterization, we prepared ten oriented thin sections of fault rocks and fault-related veins. These sections were analyzed using a Motic microscope equipped with a Nikon camera and NIS processing software, as well as a Zeiss EVO MA10 SEM, both located at the CNR-IGAG laboratories.

To determine the mineralogy of fault-related veins, we analyzed 15 vein samples through X-ray diffraction (XRD) analysis (Table S2). The whole rock samples were examined using a Bruker D8 Advance X-ray system with a Lynxeye XE-T silicon-strip detector at the Department of Earth Sciences, Sapienza University of Rome. The instrument operated at 40 kV and 30 mA with CuKα radiation (λ = 1.5406 Å). Samples were

scanned between 2 and 70° 2θ with step sizes of 0.02° 2θ, while spinning the sample to ensure even exposure. Data collection used a variable slit mode to maintain a constant irradiated area on the sample surface.

4. Results

4.1. Field mapping

The study area comprises Miocene (5.3–11 Ma) Kaldakvisl basaltic lava flows intercalated with volcaniclastic deposits, and the Breidavik Group (<1.2 Ma), consisting of glacial deposits, sandstones, shales, and conglomerates (Fig. 1 and S1-S3) (Sæmundsson and Karson, 2006). The Kaldakvisl lava flows form a gently NNE-to ENE-dipping monocline (Figs. S1 and S2), while the Breidavik Group deposits rest unconformably atop the lava flows, dipping gently towards N-NNE and SSW to SE (Fig. S3). The Kaldakvisl lavas are cut by subvertical, NW- to NE-striking, fine-grained basaltic dikes (Figs. S1–S3), with apparent horizontal thicknesses between ~1 and ~10 m.

Subsidiary faults associated with the principal Húsavik-Flatey Fault exhibit both extensional and strike-slip kinematics (Fig. 1). Normal faults strike NW, WNW, or N (Fig. 1, S1-S3). A NW-striking, SW-dipping normal fault juxtaposes the Breidavik Group sandstones and conglomerates in the hanging wall over the Kaldakvisl lavas in the footwall (Fig. S3). Dextral transtensional to strike-slip faults strike N or NW (Fig. 1, S1, and S3). Some faults display an apparent normal sense of movement and strike NW, NE, N, or E (Figs. S1–S3). NW- and N-striking apparent normal faults cut across the Breidavik Group sandstones and conglomerates. Subvertical strike-slip faults with undefined motion are mainly NNW-, ENE-, or NE-striking (Figs. S1–S3).

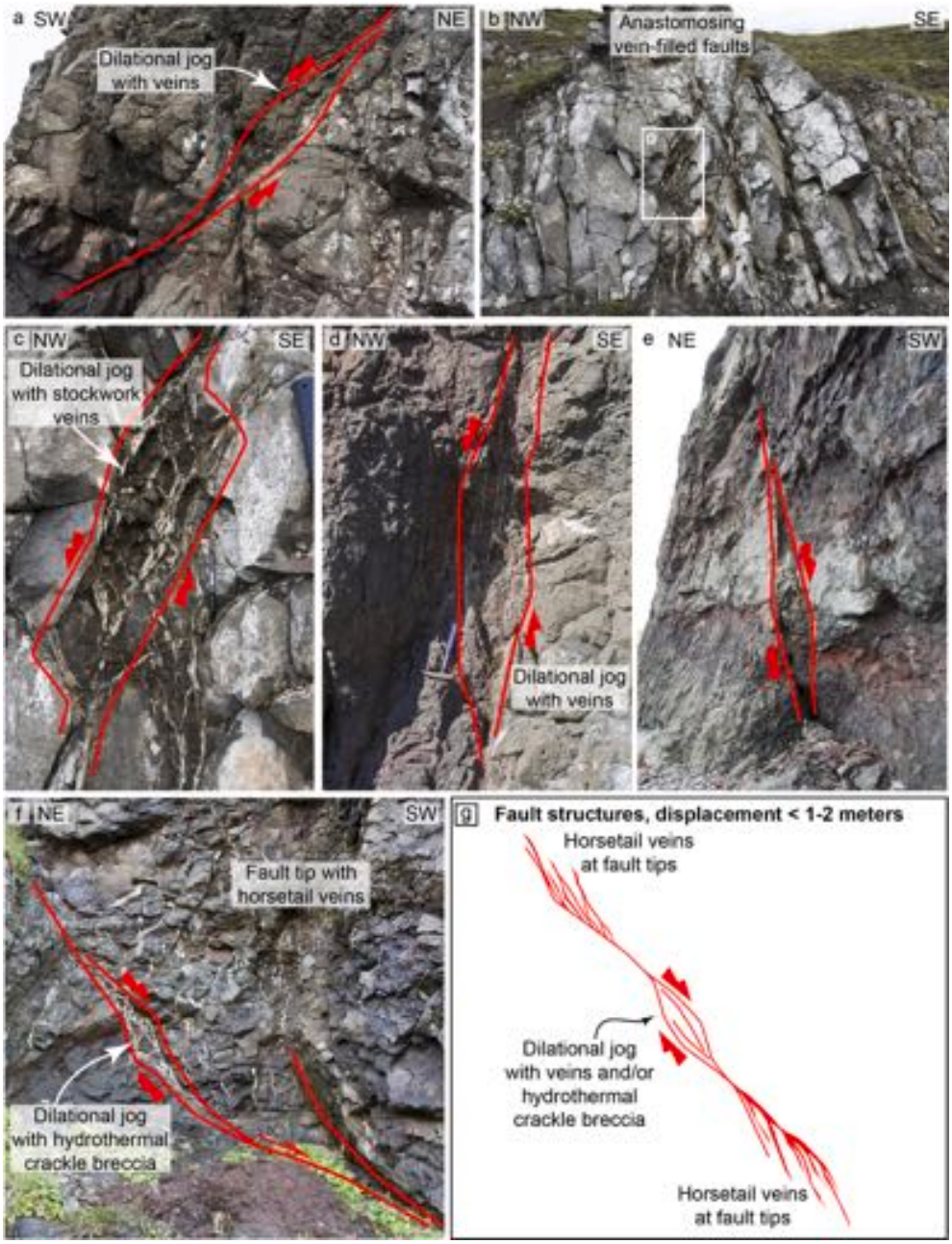

Fig. 2. Normal-transtensional faults with displacements <1–2 m are characterized by vertical overlapping fault segments connected by dilational jogs, that are crosscut by fractures, zeolite-filled veins, and hydrothermal crackle breccias **(a–f)**. Horsetail veins occur at fault tip **(f)**. In places, fault systems show anastomosed geometry **(b)**. Veins in dilational jogs can show stockwork pattern **(c)**. Schematic model of fault zone structure for displacement < 1–2 m **(g)**.

4.2. Architecture of faults and dikes

Our field study focused on faults with clear normal and transtensional kinematics, which are well-exposed in vertical cliffs. These faults exhibit displacements ranging from less than 1–2 m to a few tens of meters (Figs. 2–5). Associated veins and breccia cements are predominantly mineralized by zeolite minerals (Table S1). Faults with displacements of less than 1–2 m display undulating surfaces with dilational jogs and horsetail terminations (Fig. 2a–g and 3a,b). Dilational jogs are intersected by fractures and veins (Fig. 2a–g), often showing stockwork textures. Crackle to chaotic hydrothermal breccias (Woodcock and Mort, 2008) occur in dilational jogs (Fig. 2g). Fault tips are characterized by horsetail veins branching from the principal fault (Fig. 3a and b). Hydrothermal veins and breccias are characterized by disseminated host rock clasts and reworked vein pieces suspended in zeolite cement (Fig. 3b–e,f,g). Hydrothermal breccias occur in horsetail zones and fault damage zones (Fig. 3b), while hydrothermal veins occur along fault planes (Fig. 3e).

Faults with displacements between 2 and 10 m exhibit brecciated fault cores (Fig. 4a–f) and/or thin cataclastic layers (Fig. 4e). In some places, breccias are foliated (Fig. 4e and f), whereas reddish volcaniclastic interlayers are sheared and smeared along some fault planes (Fig. 4f).

At Hédinshöfdi, a left-lateral transtensional fault with displacements of several tens of meters is characterized by a sharp, polished principal slip surface (Fig. 5a–e), and subsidiary faults and breccia zones in the hanging wall and footwall damage zones, each a few meters thick (Fig. 5a–d). Volcaniclastic interbeds are smeared along the principal slip surfaces, forming discontinuous layers or mixing into fault breccias (Fig. 5a–d). Smeared volcaniclastic rocks are strongly foliated and exhibit slip surfaces (Fig. 5g and h).

Basaltic dikes crosscutting the Kaldakvisl lava flow are intensely veined, while the hosting lavas show little to no veining (Fig. 6a–h). Veins in the dikes show a stockwork texture (Fig. 6b–g) and chaotic breccia textures, characterized by host rock clasts suspended in the breccia cement (Fig. 6f). Dike-host rock boundaries often show slickenlines, indicating shearing and faulting (Fig. 6g and h). Shear zones are also present within the dikes (Fig. 6b).

4.3. Fault microstructures

Microstructural analyses revealed distinct features in hydrothermal breccia from the damage zone of a low-displacement (<1–2 m) fault (Fig. 3f) and in proto-cataclasite and cataclasite (Fig. 4e and f) from sharp fault planes of a fault with >10 m displacement at Hédinshöfdi (Fig. 5a). Hydrothermal veins and breccias contain angular basalt clasts

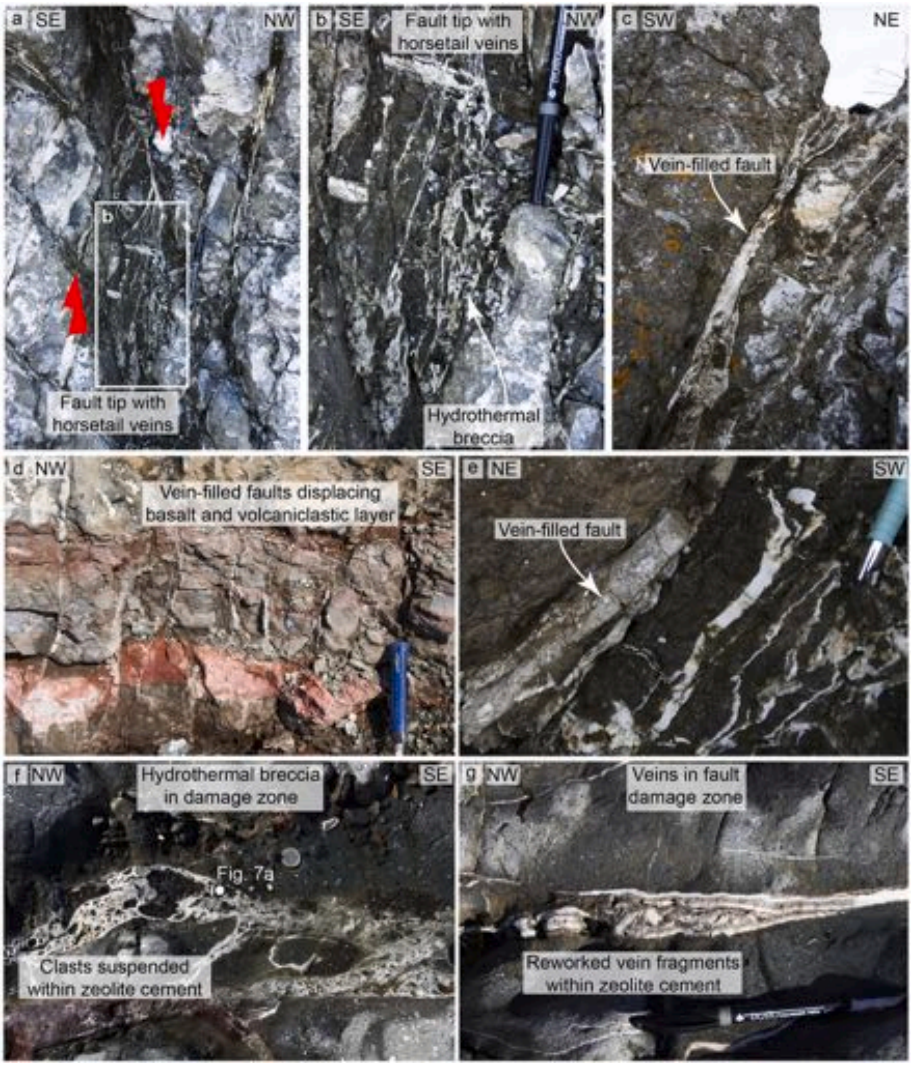

Fig. 3. Normal-transtensional faults with displacements <1–2 m are characterized by horsetail veins **(a)** and hydrothermal breccias with clasts suspended in zeolitic cement **(b)**. In places, fault planes host fault-parallel veins **(c–e)**. Hydraulic breccias and veins in the fault damage zone are characterized by host-rock clasts or reworked vein fragments suspended within breccia cement formed by zeolite minerals **(f,g)**.

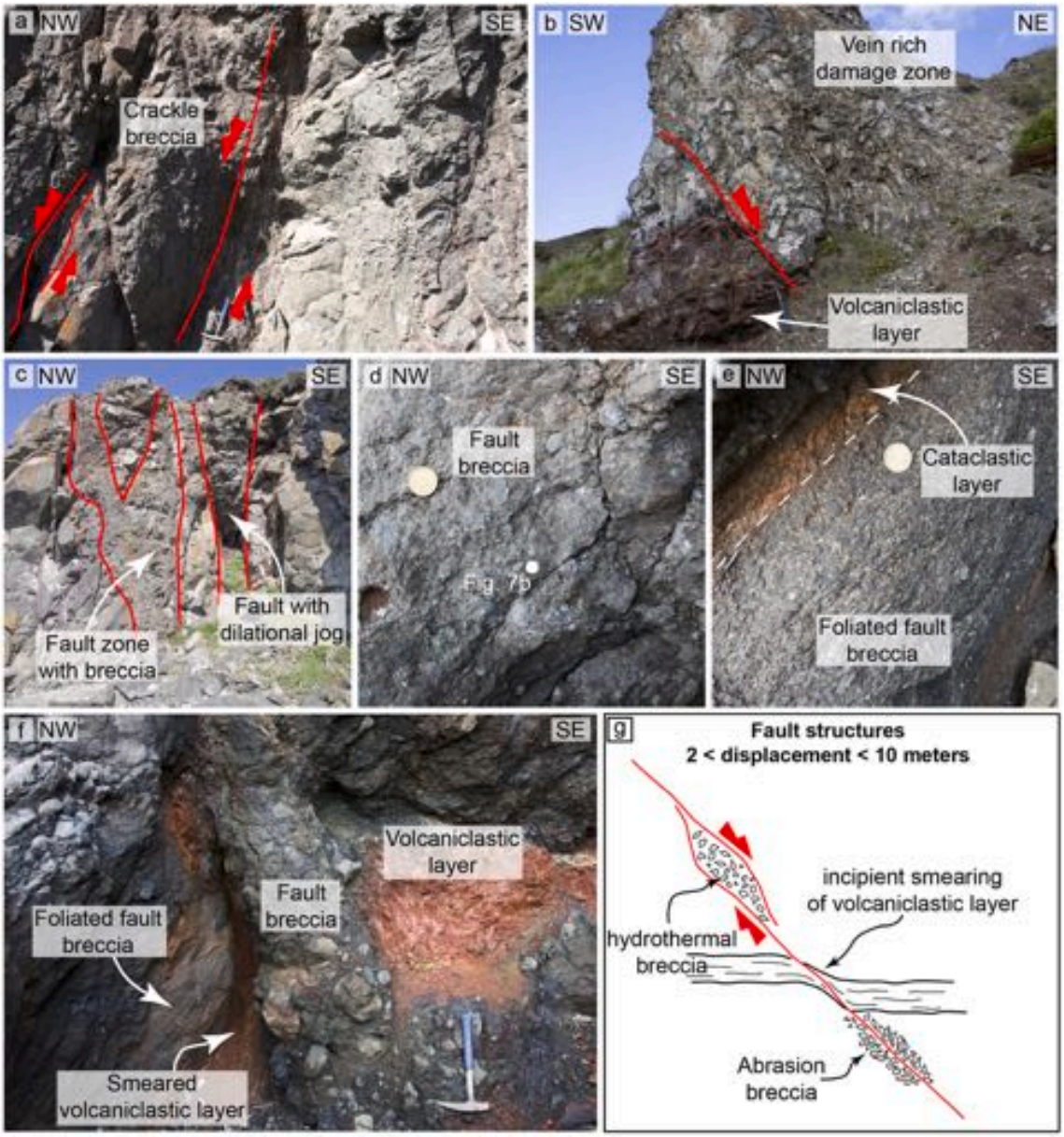

Fig. 4. Normal-transtensional faults with displacements between 2 and 10 m are characterized by: crackle breccia **(a)**, intensely veined fault damage zone **(b)**, brecciated fault cores **(d–f)**, in places foliated **(e,f)**, and thin cataclastic layers **(e)**. Interlayers of reddish volcaniclastic sandstones/shales can be sheared and smeared along the fault planes **(f)**. Schematic model of fault zone structure for displacement >2 m and <10 m **(g)**.

within a zeolite cement (Fig. 7a). Proto-cataclasite comprises angular to sub-angular basaltic clasts in a fine-grained matrix of crushed basalts (Fig. 7b). Cataclasite includes a few sub-rounded to rounded clasts of plagioclase and hornblende crystal fragments in a reddish fine-grained basalt matrix (Fig. 7c). The sharp fault plane features a 1–2 mm thick ultracataclastic layer with rounded basaltic clasts in a fine-grained matrix (Fig. 7d) composed of fine basalt fragments or clay-sized material (Fig. 8a–h). Ultracataclasite can display multiple parallel layers of varying colors or foliated and non-foliated layers (Fig. 7e and f and 8a-c, e). Contacts between ultracataclasite and host rock can be sharp (Fig. 7d–f and 8a,d), also with truncated clasts (Fig. 8b). Clay minerals of foliated ultracataclasite wrap, at places, basaltic clasts (Fig. 8g and h), generating structures resembling those of mantled clasts (sensu Passchier and Trouw, 2005).

4.4. X-ray diffraction

The X-ray diffraction analysis results are summarized in Table S2, with related spectra presented in Figs. S4 and S5. Stockwork veins in dikes are predominantly characterized by zeolite assemblages such as mesolite, stilbite, and chabazite (samples HU30, HU56), and occasionally laumontite (samples HU9 and HU19). Veins and breccia cements (samples HU11, HU14, HU54) associated with normal-transtensional faults primarily contain mesolite ± stilbite and laumontite. Fault-parallel veins with scattered host rock fragments are cemented by a single mineral such as laumontite (sample HU52), mesolite (sample HU10), or a zeolite assemblage of mesolite, chabazite, and laumontite (sample HU21).

Faults through basalts are mineralized by laumontite (sample HU4), whereas those through interlayered volcanoclastic layers exhibit a variety of zeolite-rich mineralizations such as stilbite, chabazite, and thomsonite (sample HU31), or mesolite and laumontite (sample HU36).

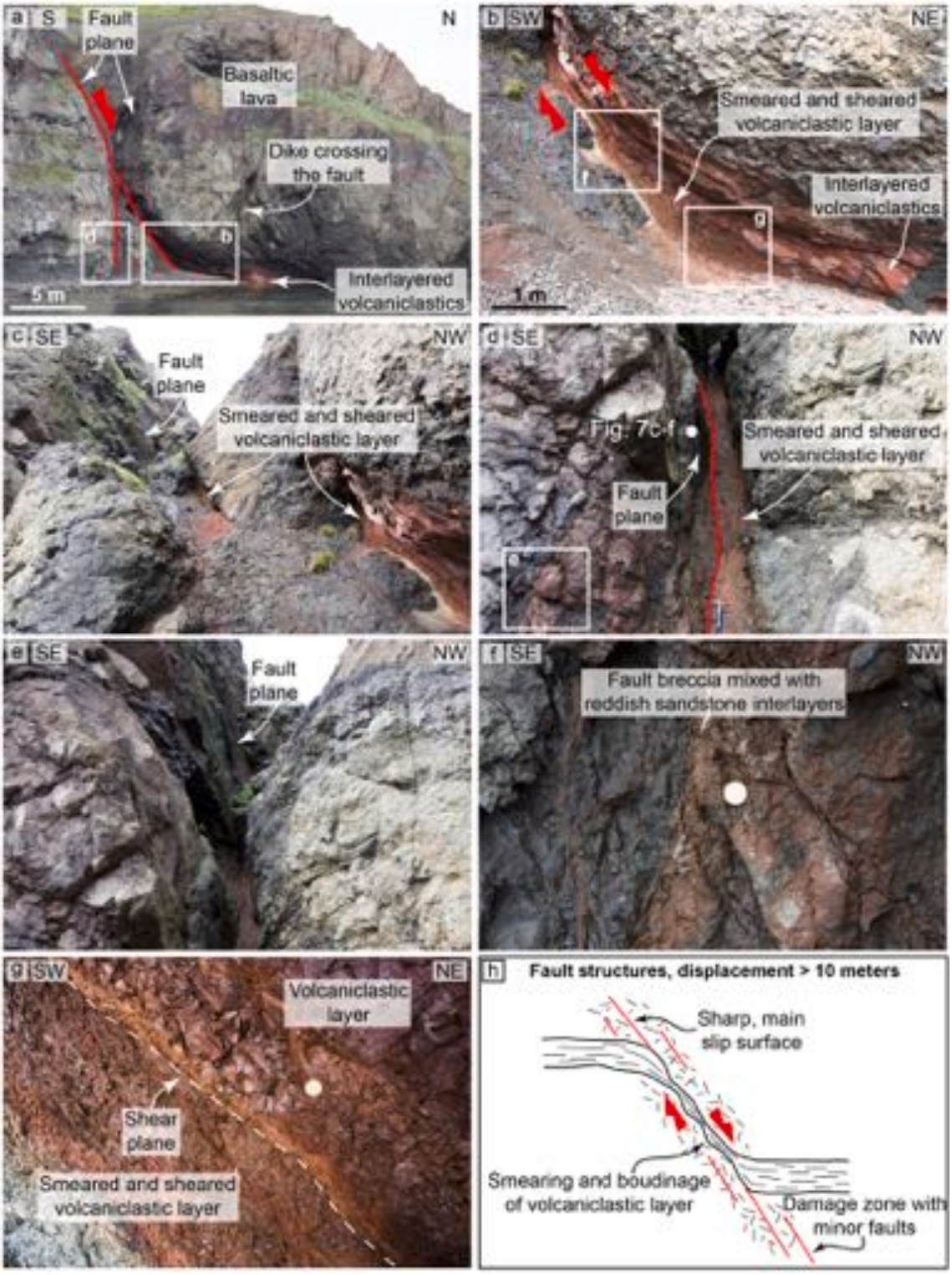

Fig. 5. The transtensional fault at Hédinshöfdi, showing displacements in the order of a few tens of meters up to potentially a hundred of meters, is characterized by a sharp principal slip surface **(a–c)**, interlayers of reddish volcaniclastic sandstones/shales sheared and smeared along the fault plane **(b–g)** and mixed within fault breccia **(d–e)**. Schematic model of fault zone structure for displacement >10 m **(h)**.

Veins along strike-slip faults (sample HU60) contain chabazite, wairakite, and analcime, whereas faults through sandstones and conglomerates (sample HU29) are characterized by calcite with negligible laumontite (1%). A similar mesolite, laumontite, and thomsonite assemblage was also identified by Wästeby et al. (2014) in veins from the Húsavik-Flatey fault damage zone.

Some X-ray tracings display a small and broad peak at low diffraction angles (about 6° 2θ), which has been interpreted as clay minerals (smectite or mixed-layer minerals) formed during glass alteration (Aldega et al., 2009) or as corresponding to basalt minerals (e.g., plagioclase), indicating host rock contamination.

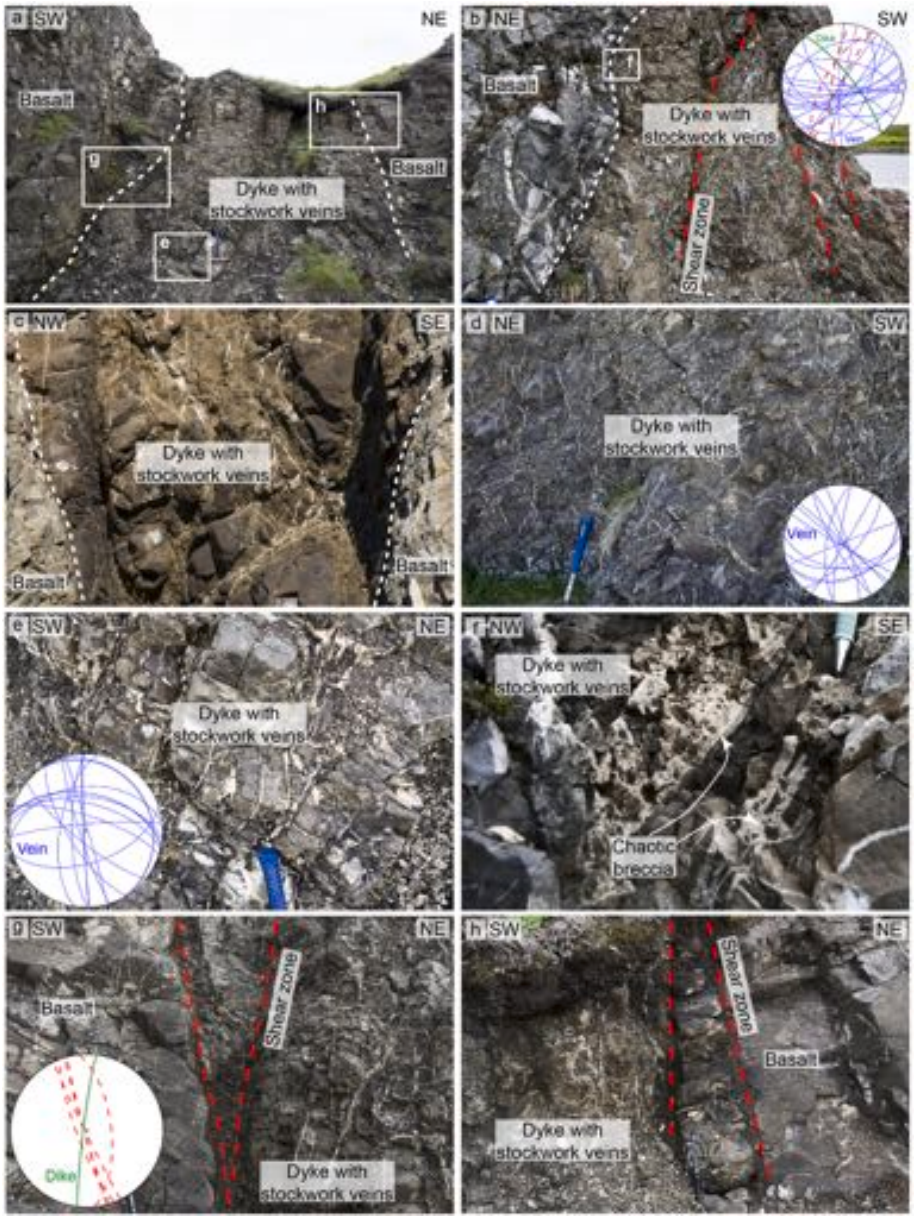

Fig. 6. Mesoscale structures within the dikes crosscutting the Kaldakvisl lavas. Generally the dikes are intensely veined (frequently with stockwork texture), while the hosting lavas show no or limited veining **(a-e,g,h)**. Chaotic breccia texture, with host rock clasts disseminated within the breccia cement, can be observed in the dikes **(f)**. The dike walls are sheared and faulted **(g,h)**, although shear zones can be observed also within the dike **(b)**.

5. Discussion

5.1. Fault development in layered basalt-volcaniclastic successions

The studied faults exhibit two primary displacement types: normal and dextral strike-slip (Fig. 1). The slip vectors for normal faults indicate an E-W extension direction, consistent with the extension direction of N-striking normal faults in the Tjörnes Fracture Zone (Fig. 1; Tibaldi et al., 2016a, 2016b, 2020; Eiríksson et al., 2021). The right-lateral oblique to strike-slip faults align with the dextral strike-slip movement of the WNW-striking Húsavik-Flatey Fault (Gudmundsson, 1993; Angelier et al., 2000; Bergerat et al., 2000; Tibaldi et al., 2016a, 2016b, 2020). The coexistence of extensional and dextral transtensional to strike-slip faults supports the transform-rift junction evolution model proposed by Tibaldi et al. (2016b), who suggest a horsetail/imbricate fan of N-striking normal faults splaying from the propagating tip of the WNW-striking, dextral transtensional Húsavik-Flatey Fault. Local stress variations at the tip of a propagating transtensional fault can indeed generate normal faults. The NW- and N-striking normal faults that cut across the Pleistocene sandstones and conglomerates of the Breidavik Group suggest they are the youngest faults in the area.

The following discussion focuses on normal-oblique faults, which are best exposed in vertical cliffs cutting perpendicularly to the fault strike. These faults exhibit various deformation mechanisms, providing fossil snapshots of normal-transtensional fault geometry and deformation mechanisms at different displacement increments.

Faults with displacements of <1–2 m typically feature overlapping fault segments connected by dilational jogs (Fig. 2a–g), similar to other low-displacement basalt-hosted faults (Walker et al., 2013a; Liotta et al., 2021) or dilatant normal faults cutting through heterogeneous sedimentary successions (Ferrill et al., 2003). Horsetail terminations at the tips of low-displacement faults show upward or downward steepening (Fig. 2g and 3a,b), indicative of shallow crustal deformation reflecting low lithostatic load and low differential stress. This is common in

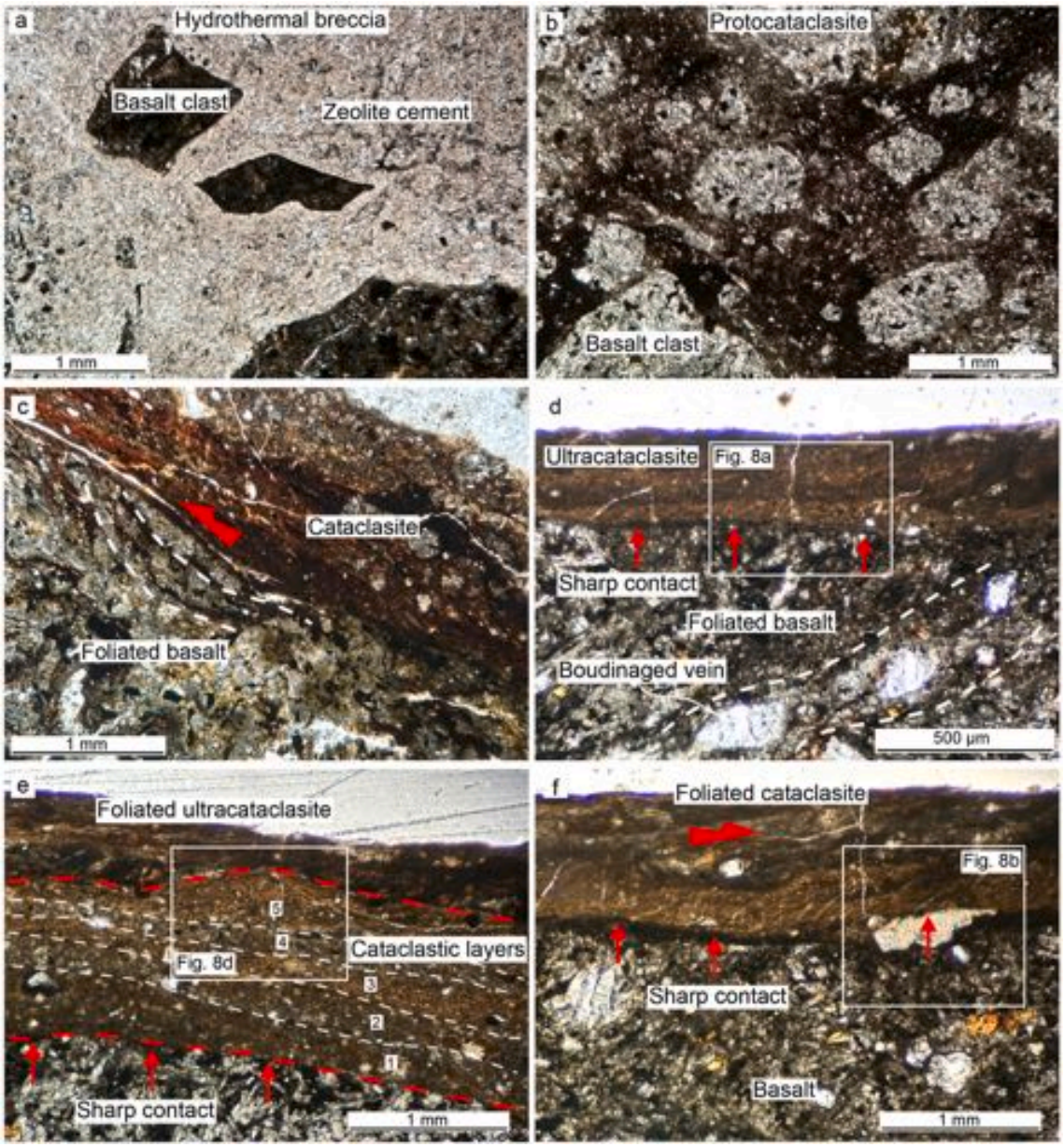

Fig. 7. Microstructures of hydrothermal breccias and different cataclasite types. **(a)** Zeolite cemented hydrothermal breccia with suspended (i.e. clasts not touching each other) sub-angular to angular basaltic host rock clasts. **(b)** Proto-cataclasite with host rock basaltic clasts scattered within matrix (<50% in total volume). **(c)** Cataclasite, **(d)** ultracataclasite, and **(e,f)** foliated cataclasite along a slip surface from the fault of Fig. 5, showing sharp contacts with the underlying, less deformed host basalt.

normal-transtensional basalt-hosted faults developed at shallow burial depths in Iceland (Kettermann et al., 2019; Von Hagke et al., 2019; Weismüller et al., 2019).

Faults with displacements between 2 and 10 m are characterized by breccias and thin cataclastic layers along the slip surfaces (Fig. 4a–f), indicating the activation of cataclastic processes. Volcaniclastic layers can be smeared along the slip surfaces (Fig. 4f). The fault at Hédinshöfdi, with displacement >10 m, shows a continuous principal slip surface with associated subsidiary slip surfaces, indicating shear localization with increasing displacement, and 4–5 m thick breccia layers in the damage zone (Fig. 5a–d). The discontinuous volcaniclastic material along the principal slip surface (Fig. 5a–d) suggests ductile drag and smearing processes of volcaniclastic interbeds. Sharp shear planes and strong foliation in smeared volcaniclastic material (Fig. 5g) suggest brittle-ductile deformation processes. Fault breccias are also characterized by a red volcaniclastic matrix, indicating mixing between basaltic breccia clasts and volcaniclastic material (Fig. 5f).

The described features of these faults can be conceptualized through progressive evolutionary stages of an individual normal fault with displacements ranging from <1 to 2 m to several tens of meters. We propose a conceptual model for fault evolution at depths <1.5 km cutting interlayered basalt-volcaniclastic sequences (Fig. 9a–c).

(a) Initial Phase (Displacement <1–2 m): Propagating and overlapping faults, probably originating along former cooling joints in basalts optimally oriented with the local stress field, generate undulating faults characterized by dilational jogs (Fig. 9a).
(b) Intermediate Phase (2 m < Displacement <10 m): Pre-existing faults connect and cataclastic processes begin. Crackle breccias form between overlapping faults (Fig. 4a), and breccias and thin cataclastic layers develop in the fault core (Fig. 4c–e,f and 9b).

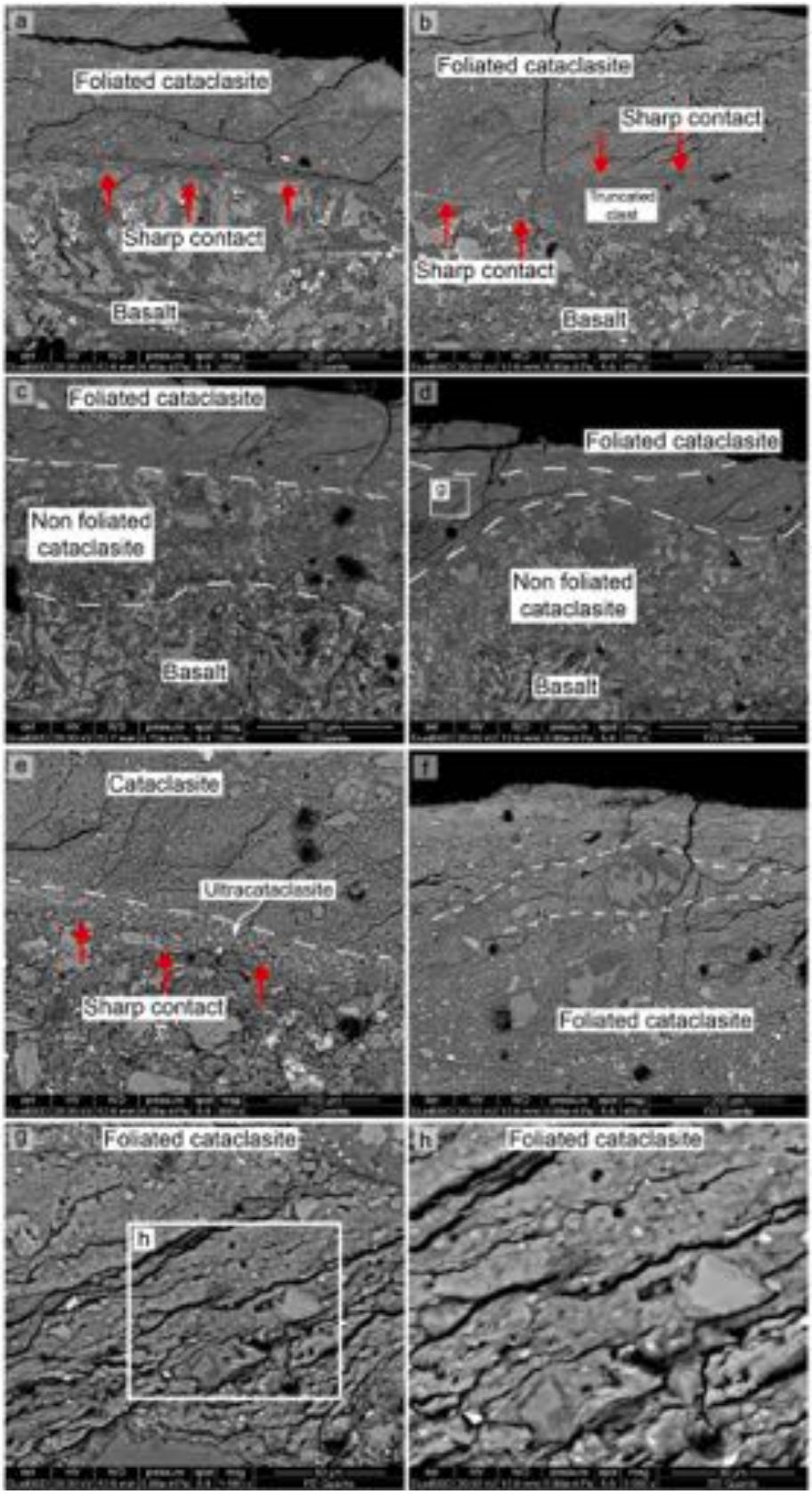

Fig. 8. Microstructures of the principal slip surface from the fault at Hédinshöfdi (Fig. 5). **(a–e)** Foliated and non-foliated cataclasites with basalt clasts scattered within a clay-rich matrix and showing diffuse to sharp contact, **(b)** in places with truncated clast, with the underlying less deformed host basalt. **(f)** Detail of basalt clasts wrapped around by clay and cataclastic material, with structure similar to that of mantled clasts (sensu Passchier and Trouw, 2005). **(g,h)** Clay minerals aligned parallel to cataclasite foliation planes and wrapping around scattered basaltic clasts.

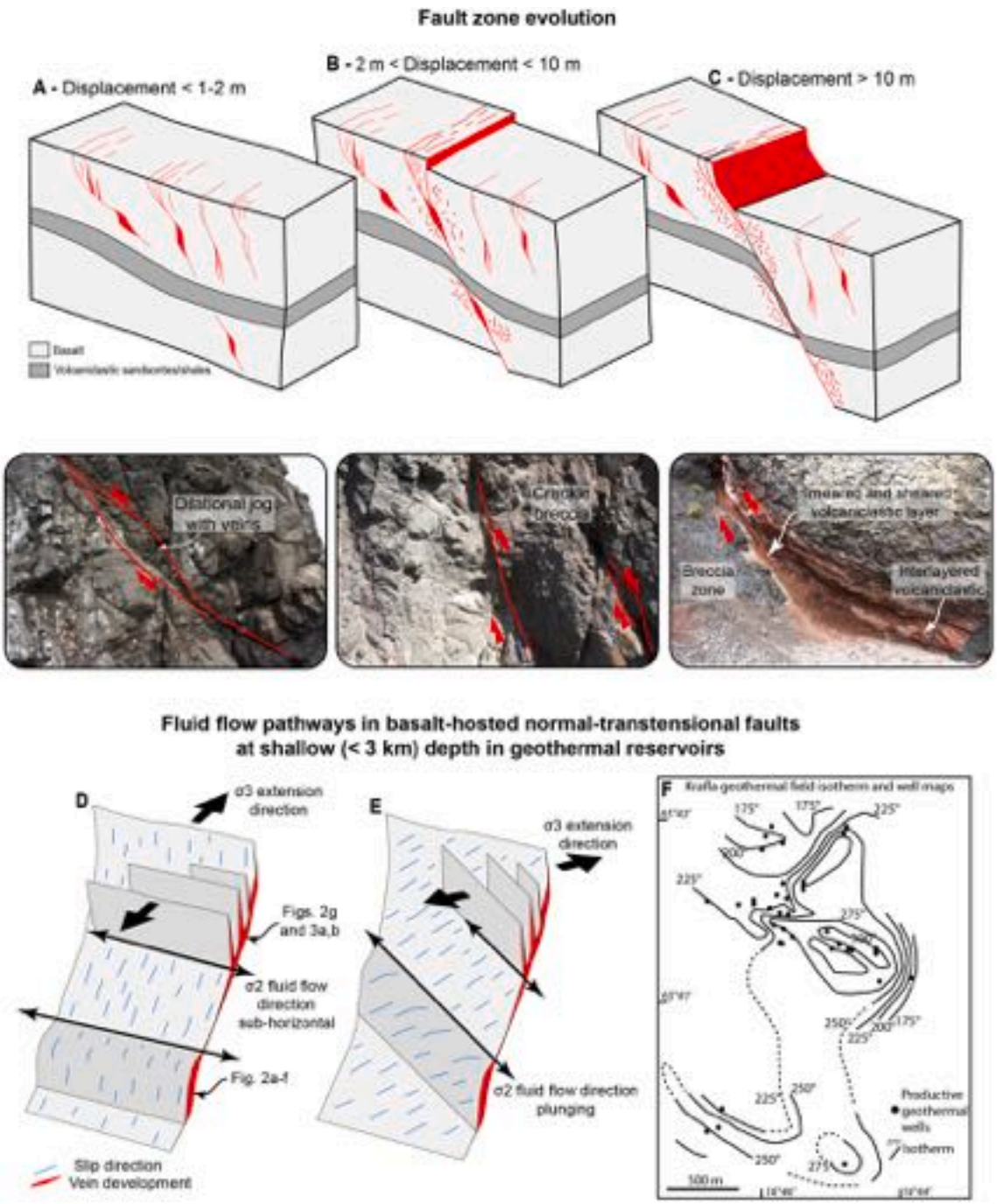

Fig. 9. **(a–c)** Schematic block diagrams illustrating fault zone evolution in layered basaltic-volcaniclastic succession. **(d,e)** Schematic block diagram illustrating fluid flow direction controls in faulted basalt at shallow depths (<1.5 km) in potential geothermal reservoirs. Modified from Rhys et al. (2020). **(f)** Geological-structural map of the Krafla active geothermal system, productive wells, and isotherms. Modified from Liotta et al. (2021).

Initial smearing of volcaniclastic material from nearby volcaniclastic interbeds occurs (Fig. 4f).

(c) Advanced Phase (Displacement >10 m): Breccias form up to ~4–5 m thick tabular zones in the damage zone. Shear displacement localizes along a principal slip surface and subsidiary slip planes in the damage zone (Fig. 5a–d and 9c). Increasing displacement results in further smearing of volcaniclastic interbeds along the fault core, potentially becoming discontinuous (Fig. 5a–d and 9c). This smearing process is also observed in basalt-hosted faults with displacement >1 m crosscutting basaltic-volcaniclastic successions in the Faroe Islands (Walker et al., 2011, 2013a) and is similar to processes in faulted sedimentary successions characterized by alternating shale-sandstone or marl-limestone (Vrolijk et al., 2016 for a review). This fault development model aligns with previously proposed models for basalt-hosted fault development in the Faroe Islands (Walker et al., 2011, 2012, 2013a, 2013b; Bamberg et al., 2022).

5.2. Implications for hydrothermal fluid flow in geothermal reservoirs

The studied faults developed at depths of less than 1.5 km (Sæmundsson and Karson, 2006). The presence of zeolites such as stilbite, mesolite, chabazite, and laumontite in veins and breccia cements

indicates fluid circulation at temperatures ranging from ~25 °C to 230–260 °C (Kristmannsdottir and Tómasson, 1978; Weisenberger and Selbekk, 2009). This suggests that the studied faults may represent tectonic structures that develop in low to high-enthalpy basalt-hosted shallow geothermal systems located in extensional-transtensional tectonic settings. Active basalt-hosted geothermal systems in such settings are currently exploited or explored in regions like Iceland (Arnorsson, 1995), the Faroe Islands (Eidesgaard et al., 2019), Greenland (Hjartarson and Ármannsson, 2010), the USA (Faulds et al., 2010), Ethiopia (Didana and Heinson, 2015), and India (Kumar and Thiagarajan, 2011).

Field data show that faults with displacements of less than 1–2 m are heavily mineralized with zeolite veins or hydrothermal breccias, mostly located in dilational jogs or at fault tips and horsetail veins (Fig. 2a–h and 3a-d). This suggests that past fluid flow was localized in low-displacement faults due to their dilatant behavior at shallow depths. Slip along fault jogs, bends, geometric irregularities, and orientation changes causes the dilatant opening of the fault planes and extensional horsetail fractures at fault tips (Sibson, 1996; Rhys et al., 2020). These structures create main tabular zones for lateral movement of hydrothermal fluids, parallel to the fault strike. Additionally, the dilational jogs and the intersection of horsetail veins with the hosting faults may define linear zones of high structural permeability and intense localized fluid flow and mineral precipitation, as observed in fossil geothermal systems and epithermal mineral deposits (Sibson, 1996; Rhys et al., 2020). This intersection is parallel to the σ2 paleostress orientation and perpendicular to fault movement (Sibson, 1996; Rhys et al., 2020; Liotta et al., 2021). Such linear zones have different plunges based on fault kinematics. For normal faults, the linear zone is sub-horizontal, promoting lateral fluid movement (Fig. 9d). In transtensional faults, the linear zone is gently to moderately dipping, facilitating the ingress of fluids from reservoirs located above and/or below the fault (Fig. 9e).

Therefore, shallow geothermal reservoirs in extensional-transtensional tectonic settings with low-displacement and dilatant normal or transtensional faults may be characterized by sub-horizontal to gently-moderately plunging pathways of enhanced hydrothermal fluid flow. The circulation of hot hydrothermal fluids is consistent with the presence of minerals like wairakite, analcime, and laumontite in fault-related mineralizations (Table S1), indicating fluid temperatures above 100 °C and below 230–260 °C (Kristmannsdottir and Tómasson, 1978; Weisenberger and Selbekk, 2009) within fault zones developed at depths less than 1.5 km (Sæmundsson and Karson, 2006).

The concept of a linear zone of high structural permeability and localized fluid flow can be applied to the Krafla field, located ~50 km southeast of the study area, at the intersection of the WNW-striking Húsavik-Flatey Fault and the ~N- to NNE-striking faults of the Krafla fracture swarms (Khodhayar, 2018; Liotta et al., 2021) (Fig. 1). This zone of fault intersection is considered an efficient channel for the vertical upflow of hot to super-hot geothermal fluids (Liotta et al., 2021). The NNE-striking normal faults are favorable loci for enhanced local permeability and hydraulic conductivity (Thorsteinsdóttir et al., 2020). This can be explained by NNE-trending, sub-horizontal fluid pathways along NNE-striking dilatant normal faults, enabling the lateral redistribution of geothermal fluid. Most productive wells align along a WNW-striking trend (parallel to the Húsavik-Flatey Fault, Fig. 9f; Liotta et al., 2021), while some align along NNE-striking trends (Fig. 9f; Liotta et al., 2021), supporting the idea of NNE-trending fluid pathways. It is assumed that dilatant structures (e.g., dilational jogs and horsetail veins) observed in the studied low-displacement normal faults also occur at depth along the NNE-striking normal faults of the Krafla field. Fault connectivity at depth along dilatant basalt-hosted normal faults is also supported by analog laboratory experiments and numerical modeling (von Hagke et al., 2019; Weismüller et al., 2019).

Mineral precipitation can also seal fractures, hindering fluid flow (Moore et al., 2001; Liotta et al., 2021). Therefore, understanding the relationship between the present-day stress field and fault-fracture orientation is crucial during exploration to determine which structures remain open to fluid flow. Additionally, the fault slip history and mineral precipitation rates are also important in defining the hydraulic conductivity at depth. In a slow-sliding fault where cementation rates exceed the rate of dilation, all fractures are likely to be sealed. Conversely, in seismically active faults where cementation rates are slower than the dilation rate, fractures will likely remain open for a long time after significant slip.

In the study area, basaltic dikes intruding the layered basalt-volcaniclastic succession are heavily pervaded by stockwork zeolite veins and hydrothermal breccias (Fig. 6a–h), indicating intense past fluid flow. It is proposed that dikes, likely more competent than the hosting basalts, were prone to hydrofracturing, possibly during co-seismic release of trapped overpressured fluids (see section 5.3). Thus, in basalt-hosted geothermal reservoirs, dikes can form conduits for localized geothermal fluid flow or tabular zones for fluid storage.

The fault at Hédinshöfdi, with displacements over 10 m, shows little to no evidence of mineralization, suggesting limited or absent past fluid flow due to low permeability, clay-rich cataclasite development (Fig. 8a–h), and/or smearing and mixing of clay-rich volcaniclastic material along fault surfaces (Fig. 5a–h). This material can reduce fault permeability, creating a barrier for fluid flow across the fault, as seen in faulted sedimentary successions with alternating shale-sandstone interbeds (Vrolijk et al., 2016). Specifically, clay-rich cataclasite and smeared clay-rich volcaniclastic material can reduce across-fault permeability, while permeability parallel to the fault may remain high due to breccias and fractures in the damage zones.

Field data by Walker et al. (2013a) show that zeolite veins can occur in smeared, clay-rich volcaniclastic material. They suggest that faults with displacements over 1 m can serve as channelized pathways for fluid flow parallel to the fault due to the brittle behavior of volcaniclastic material at depths below 3 km. Porosity measurements indicate that fault rocks from low displacement (<1 m) faults have relatively low permeability (10^{-17} to 10^{-20} m^2), while those from higher displacement (>1 m) structures have comparatively high permeability (10^{-15} to 10^{-17} m^2) (Walker et al., 2013a, 2013b). The low fault permeability is attributed to the precipitation of clay minerals in low-displacement faults, whereas high permeability is attributed to fracture creation in high-displacement faults (Walker et al., 2013b). These measurements reflect fault permeability in static conditions (i.e., without fault slip). We believe that dynamic permeability creation and destruction during natural or induced seismic slip along faults in basaltic reservoirs should be properly considered when modeling the hydraulic behavior of active basalt-hosted faults (Bamberg et al., 2022, 2023) in geothermal reservoirs.

5.3. Evidence of fluid-assisted seismic cycle

Meso- and micro-structures of the studied faults and dikes provide evidence of different phases of past fluid-assisted seismic cycles. Zeolite-cemented hydrothermal crackle to chaotic breccias and filled veins in dilational jogs and horsetail fault tips (Fig. 2a–g and 3a,b) are consistent with co-seismic dilatant openings, aligning with the “suction pump" model by Sibson (2000) (Fig. 10a and b). These observations suggest that newly created voids, which are zones of extremely low pressure, cause surrounding fluids and host rock fragments to be rapidly drawn towards the fault zones. The sudden pressure drop favors the rapid precipitation of zeolite minerals, suspending clasts in the fluid (Bamberg et al., 2022, 2023). This process is consistent with the presence of angular clasts in hydrothermal breccias (Fig. 8a), which could only be preserved if transport-related wear was minimal and zeolite precipitation was nearly instantaneous. Reworked veins and hydrothermal breccia fragments (Fig. 3f and g) indicate multiple events of co-seismic dilation, fluid flow, and zeolite precipitation.

Low-permeability clays typically develop in damage zones of basalt-hosted faults with displacements less than 1 m, in fault cores of basalt-

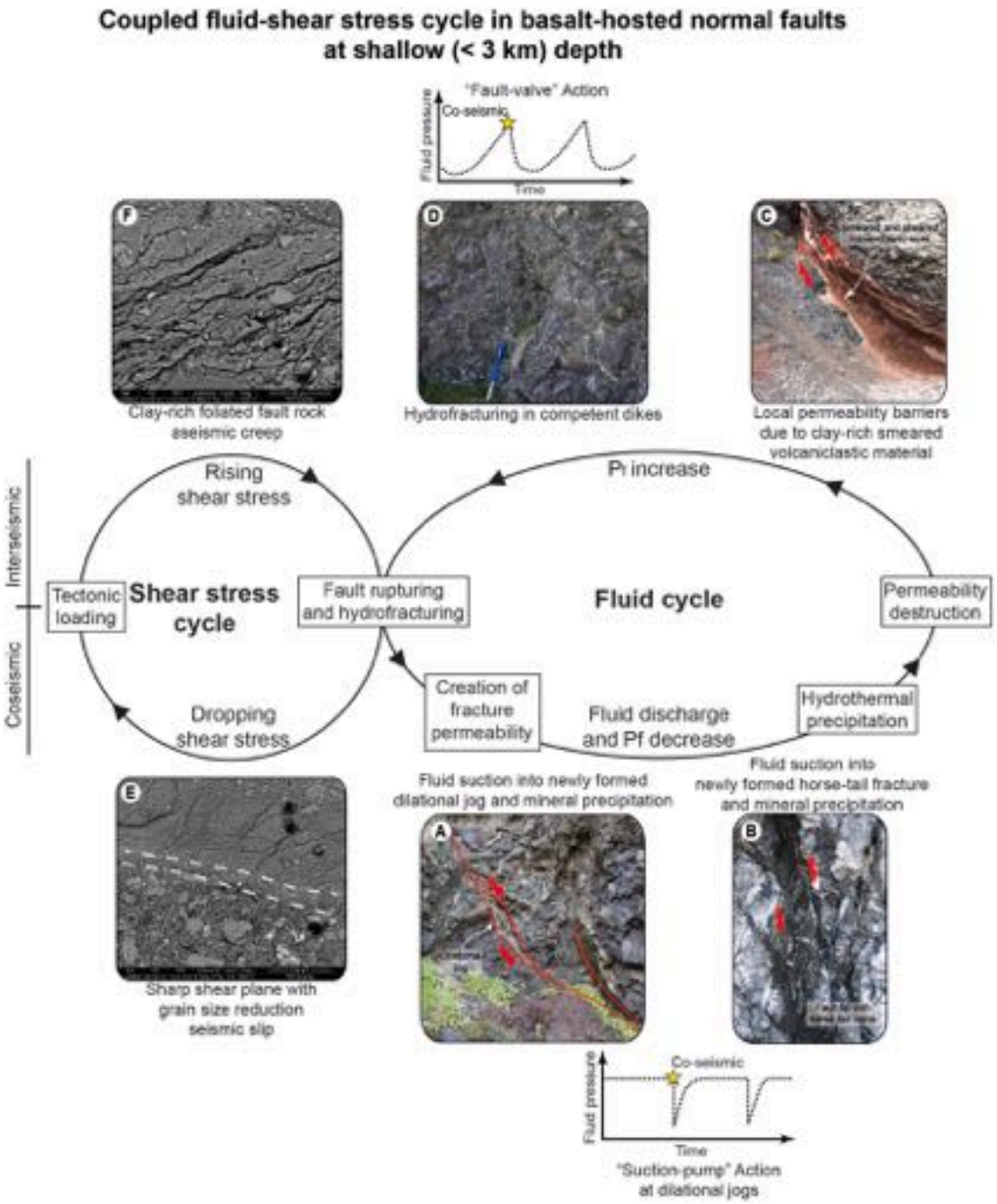

Fig. 10. (a–f) Coupled fluid-shear stress cycle in basalt-hosted normal faults at shallow (<3 km) depth, following the "suction-pump" and "fault-valve" models of Sibson (2000). Modified from Sibson (1994, 2000).

hosted faults with displacements greater than 1 m due to clay redistribution (Walker et al., 2013b; Bamberg et al., 2023), and in basalt-hosted faults with displacements greater than 10 m due to clay smearing (Walker et al., 2013b). This was also observed along the fault at Hédinshöfdi (Fig. 5f–h). These fluid potential barriers may lead to cross-fault fluid compartmentalization, pore fluid trapping, and fluid pressure rise during the interseismic phase (Byerlee, 1993; Caine et al., 2010; Sutherland et al., 2012, Fig. 10c), resulting in fluid overpressure release during co-seismic slip and hydrofracturing. Stockwork veins in basaltic dikes (Fig. 6a–h) and hydrothermal veins along slip surfaces (Fig. 3e and 4c) suggest co-seismic release of overpressured fluids, following the "fault-valve" model by Sibson (2000) (Fig. 10d). Such fluid release can transiently decrease frictional strength (Faulkner et al., 2018) in velocity-weakening portions of a fault, i.e., where basalt is in contact with basalt, eventually triggering seismogenic slips. Subsequent zeolite precipitation could cement and restrengthen the slip zone, decreasing fault permeability and triggering a new fluid-earthquake cycle (Sibson, 1994; Bamberg et al., 2022, 2023) (Fig. 10). For instance, complete fracture cementation by zeolite precipitation during the interseismic phase may occur 8–10 years after a seismic slip (Wästeby et al., 2014; Bamberg et al., 2022).

Laboratory shear experiments indicate that basalt gouges exhibit velocity strengthening behavior (prone to slip aseismically) at pressures below 5 MPa (Zhong et al., 2023). The transition from velocity

strengthening to velocity weakening behavior (capable of generating seismic slip) occurs at pressures equal to or greater than 10 MPa (Giacomel et al., 2018, 2021; Zhong et al., 2023) and temperatures above 300 °C (Zhang et al., 2017). These pressure and temperature ranges are typical of shallow geothermal reservoirs (Arnorsson, 1995) or CO_2 sequestration and storage sites in basalt, such as the Carbfix CO_2-injection facilities in Iceland (Oelkers and Gislason, 2023). The transition from velocity strengthening to velocity weakening behavior is associated with shear localization along sharp slip surfaces, characterized by intense grain size reduction compared to the surrounding cataclasite (Giacomel et al., 2021; Zhang et al., 2017). In contrast, the velocity strengthening behavior in basalt-hosted faults is linked to the presence of clay minerals coating the rims of large and strong basalt grains (Ikari et al., 2020), consistent with the behavior observed in clay-rich sedimentary fault rocks (e.g., Boulton et al., 2014; Tesei et al., 2014).

Our structural and microstructural evidence from the principal slip zone of the fault at Hédinshöfdi reveals both velocity weakening-related structures, such as shear localization with intense grain size reduction along sharp slip surfaces (Fig. 7d,e, 8a-e), and velocity strengthening-related structures, such as clay-rich foliated cataclasite (Fig. 8a–h).

These inferences are further supported by comparisons with meso- and micro-structures observed in other fault rock types. Foliated breccias (Fig. 4e) and foliated clay-rich cataclasites (Fig. 8a–h), observed in basalt-hosted faults, resemble those found in carbonate- or clay-rich-hosted faults, which develop during slow aseismic creep (Tesei et al., 2014; Vignaroli et al., 2020). Conversely, the presence of truncated clasts along sharp slip surfaces (Fig. 8b) may indicate past seismic slip, similar to laboratory experiments in carbonate gouges showing that truncated clasts form during seismic slip rates (Fondriest et al., 2013). Mantled clasts (Fig. 8f) can represent both aseismic (Smeraglia et al., 2017) and seismic slips (Smith et al., 2011; Rempe et al., 2014). Similar structures have been observed in basalt-hosted faults with displacements greater than 10 m in the Faroe Islands (Walker et al., 2013a, 2013b; Bamberg et al., 2022).

The discussion above suggests that basalt-hosted faults with tens of meters of displacement likely accommodated cycles of seismic slips and aseismic creep (Fig. 10e and f), akin to mechanically heterogeneous fault zones in sedimentary successions or tectonic mélanges. These fault zones consist of velocity strengthening layers rich in clay (prone to aseismic slip) and velocity weakening layers in more competent rocks (capable of generating seismic slips) (Tesei et al., 2014; Volpe et al., 2022, 2023).

6. Conclusions

We integrated structural and microstructural observations with X-Ray diffraction analyses on exposed normal-transtensional faults exhumed from depths less than 1.5 km and fault-related veins associated with the seismically active Húsavik-Flatey Fault in Northern Iceland. The results reveal several key insights.

First, the evolution of basalt-hosted normal-oblique faults with increasing displacement can be synthesized into sequential phases. These include low-displacement fault propagation from pre-existing cooling joints, fault linkage through dilational jogs, damage zone and fault core growth through brecciation and cataclastic processes. With increasing displacement shear localizes along sharp slip surfaces within the fault core and damage zone, and finally volcaniclastic interbeds are smeared along the principal fault plane. The smeared volcaniclastic interbeds can create cross-fault barriers for fluid circulation, promoting compartmentalized and discontinuous pockets of overpressured fluids.

Second, the studied faults show evidence of multiple, fluid-assisted seismic cycles. Features such as shear localization with intense grain size reduction, truncated clasts, and hydrothermal breccias/veins suggest multiple episodes of seismic slip assisted by pressurized fluids, consistent with the “suction pump” or “fault valve” behaviors. Conversely, clay-rich foliated cataclasite indicates aseismic slips during interseismic phases. Specifically, the occurrence of smeared, clay-rich fault rocks along slip planes can promote velocity strengthening behavior and aseismic slips, while the transition from velocity strengthening to velocity weakening behavior can be associated with localization along slip surfaces and grain size reduction relative to the surrounding cataclasite.

Third, the zeolite assemblage of stilbite, mesolite, chabazite, and laumontite in fault-related veins and breccia cements suggests fluid circulation at temperatures between approximately 25 °C and 230 °C. Therefore, the studied faults may represent tectonic structures that develop in low to high-enthalpy basalt-hosted geothermal systems located in extensional-transtensional tectonic settings.

Fourth, slip along fault jogs, bends, geometric irregularities, and fault orientation changes causes the dilatant opening of fault planes and extensional horsetail fractures at fault tips. These structures create main tabular zones for lateral movement of hydrothermal fluids parallel to the fault strike. Additionally, the dilational jogs and the intersection of horsetail veins with the hosting faults may define linear zones of high structural permeability and intense, localized fluid flow parallel to the σ2 paleostress orientation, promoting mineral precipitation. Sub-horizontal to gently plunging linear pathways can facilitate the lateral movement of hydrothermal fluids within a geothermal reservoir, while moderately plunging linear pathways can promote the upflow of deep, hot hydrothermal fluids into the reservoir.

Lastly, basalt-hosted faults can be prone to both seismic and aseismic slips. Pockets of overpressured fluids may be generated where low-permeability clay-rich volcaniclastic material is smeared along slip surfaces. Seismic slip may be triggered by overpressured fluids if the fluid compartment is breached, along velocity-weakening (i.e., prone to slip seismically) portions of the same fault characterized by intense basalt grain size reduction. Conversely, portions of the same fault with smeared clays may exhibit velocity strengthening behavior (i.e., prone to slip aseismically). Understanding basalt-hosted fault slip behaviors is crucial for better modeling induced seismicity in basalt reservoirs, both for enhanced geothermal fluid recovery or industrial CO_2 storage and sequestration, and for improved borehole planning during geothermal fluid extraction.

CRediT authorship contribution statement

Luca Smeraglia: Writing – original draft, Validation, Methodology, Investigation, Formal analysis, Data curation, Conceptualization. **Andrea Billi:** Writing – review & editing, Validation, Investigation, Funding acquisition, Formal analysis, Data curation, Conceptualization. **Eugenio Carminati:** Writing – review & editing, Validation, Investigation, Funding acquisition, Formal analysis, Data curation, Conceptualization. **Luca Aldega:** Writing – review & editing, Validation, Methodology, Investigation, Formal analysis, Data curation. **Alasdair Skelton:** Writing – review & editing, Validation. **Gabrielle Stockmann:** Writing – review & editing, Validation. **Erik Sturkell:** Writing – review & editing, Validation.

Declaration of generative AI and AI-assisted technologies in the writing process

During the preparation of this work the author(s) used ChatGPT in order to improve readability and fluency. After using this tool/service, the author(s) reviewed and edited the content as needed and take(s) full responsibility for the content of the publication.

Declaration of competing interest

The authors declare that they have no known competing financial interests or personal relationships that could have appeared to influence the work reported in this paper.

Data availability

Data will be made available on request.

Acknowledgements

Financial support by Fondazione ANIA (www.fondazioneania.it) (A. Billi), the Italian Ministry of University, and Research (MUR) through PRIN project "FAST-Fault architecture in space and time" (PRIN 2020, PI G. Viola, local coordinator L. Aldega; CUP Master J33C22000170001), and by Sapienza Progetti di Ateneo 2021 (E. Carminati) is acknowledged. This study was carried out within the RETURN Extended Partnership and received funding from the European Union Next-GenerationEU (National Recovery and Resilience Plan – NRRP, Mission 4, Component 2, Investment 1.3 – D.D. 1243 2/8/2022, PE0000005). We thank the reviewers Bob Bamberg and Christoph von Hagke, and the Editor Virginia Toy for improving this manuscript with their suggestions.

Appendix A. Supplementary data

Supplementary data to this article can be found online at https://doi.org/10.1016/j.jsg.2024.105265.

References

Acocella, V., Korme, T., Salvini, F., 2003. Formation of normal faults along the axial zone of the Ethiopian Rift. J. Struct. Geol. 25 (4), 503–513.
Aldega, L., Cuadros, J., Laurora, A., Rossi, A., 2009. Weathering of phlogopite to beidellite in a karstic environment. Am. J. Sci. 309, 689–710.
Angelier, J., Bergerat, F., Homberg, C., 2000. Variable coupling across weak oceanic transform fault: Flateyjarskagi, Iceland. Terra. Nova 12 (3), 97–101.
Arnórsson, S., 1995. Geothermal systems in Iceland: structure and conceptual models—I. High-temperature areas. Geothermics 24 (5–6), 561–602.
Bamberg, B., Reichow, M.K., Walker, R.J., Ougier-Simonin, A., 2023. Petrological evolution and mass redistribution in basaltic fault zones: an example from the Faroe Islands, North Atlantic Igneous Province. G-cubed 24 (12), e2023GC011112.
Bamberg, B., Walker, R., Reichow, M., Ougier-Simonin, A., 2022. Fluid-driven cyclic reorganization in shallow basaltic fault zones. Geosphere 18 (5), 1600–1621.
Barbieri, M., Franchini, S., Barberio, M.D., Billi, A., Boschetti, T., et al., 2021. Changes in groundwater trace element concentrations before seismic and volcanic activities in Iceland during 2010–2018. Sci. Total Environ. 793, 148635.
Bergerat, F., Angelier, J., Homberg, C., 2000. Tectonic analysis of the Húsavik-Flatey Fault (northern Iceland) and mechanisms of an oceanic transform zone, the Tjörnes Fracture Zone. Tectonics 19 (6), 1161–1177.
Björnsson, A., 1985. Dynamics of crustal rifting in NE Iceland. J. Geophys. Res. 90 (NB12), 151–162.
Boschetti, T., Barbieri, M., Barberio, M.D., Skelton, A., Stockmann, G., Toscani, L., 2022. Geothermometry and water–rock interaction modelling at Hafralækur: possible implications of temperature and CO2 on hydrogeochemical changes previously linked to earthquakes in northern Iceland. Geothermics 105, 102535.
Boulton, C., Moore, D.E., Lockner, D.A., Toy, V.G., Townend, J., Sutherland, R., 2014. Frictional properties of exhumed fault gouges in DFDP-1 cores, Alpine Fault, New Zealand. Geophys. Res. Lett. 41 (2), 356–362.
Byerlee, J.D., 1993. Model for episodic flow of high-pressure water in fault zones before earthquakes. Geology 21 (4), 303–306.
Bubeck, A., Walker, R.J., Imber, J., MacLeod, C.J., 2018. Normal fault growth in layered basaltic rocks: the role of strain rate in fault evolution. J. Struct. Geol. 115, 103–120.
Caine, J.S., Bruhn, R.L., Forster, C.B., 2010. Internal structure, fault rocks, and inferences regarding deformation, fluid flow, and mineralization in the seismogenic Stillwater normal fault, Dixie Valley, Nevada. J. Struct. Geol. 32 (11), 1576–1589.
Claesson, L., Skelton, A., Graham, C., Dietl, C., Mörth, M., Torssander, P., Kockum, I., 2004. Hydrogeochemical changes before and after a major earthquake. Geology 32 (8), 641–644.
Delle Piane, C., Clennell, M.B., Keller, J.V., Giwelli, A., Luzin, V., 2017. Carbonate hosted fault rocks: a review of structural and microstructural characteristic with implications for seismicity in the upper crust. J. Struct. Geol. 103, 17–36.
Didana, Y.L., Thiel, S., Heinson, G., 2015. Three dimensional conductivity model of the Tendaho high enthalpy geothermal field, NE Ethiopia. J. Volcanol. Geoth. Res. 290, 53–62.
Eidesgaard, Ó.R., Schovsbo, N.H., Boldreel, L.O., Ólavsdóttir, J., 2019. Shallow geothermal energy system in fractured basalt: a case study from Kollafjørður, Faroe Islands, NE-Atlantic Ocean. Geothermics 82, 296–314.
Eiríksson, J., Guðmundsson, A.I., Símonarson, L.A., Einarsson, P., Hjartardóttir, Á.R., Brandsdóttir, B., 2021. The evolution of the Tjörnes sedimentary basin in relation to the Tjörnes Fracture Zone and the geological structure of Iceland. Pacific-Atlantic Mollusc Migration: Pliocene Inter-ocean Gateway Archives on Tjörnes, pp. 37–55. North Iceland.
Faulds, J., Coolbaugh, M., Bouchot, V., Moek, I., Oguz, K., 2010. Characterizing structural controls of geothermal reservoirs in the Great Basin, USA, and Western Turkey: developing successful exploration strategies in extended terranes. In: World Geothermal Congress 2010, p. 11.
Faulkner, D.R., Sanchez-Roa, C., Boulton, C., Den Hartog, S.A.M., 2018. Pore fluid pressure development in compacting fault gouge in theory, experiments, and nature. J. Geophys. Res. Solid Earth 123 (1), 226–241.
Fondriest, M., Smith, S.A., Candela, T., Nielsen, S.B., Mair, K., Di Toro, G., 2013. Mirror-like faults and power dissipation during earthquakes. Geology 41 (11), 1175–1178.
Garcia, S., Arnaud, N.O., Angelier, J., Bergerat, F., Homberg, C., 2003. Rift jump process in Northern Iceland since 10 Ma from 40Ar/39Ar geochronology. Earth Planet Sci. Lett. 214 (3–4), 529–544.
Giacomel, P., Spagnuolo, E., Nazzari, M., Marzoli, A., Passelegue, F., Youbi, N., Di Toro, G., 2018. Frictional instabilities and carbonation of basalts triggered by injection of pressurized H2O-and CO2-rich fluids. Geophys. Res. Lett. 45 (12), 6032–6041.
Giacomel, P., Ruggieri, R., Scuderi, M.M., Spagnuolo, E., Di Toro, G., Collettini, C., 2021. Frictional properties of basalt experimental faults and implications for volcano-tectonic settings and geo-energy sites. Tectonophysics 811, 228883.
Grant, J.V., Kattenhorn, S.A., 2004. Evolution of vertical faults at an extensional plate boundary, southwest Iceland. J. Struct. Geol. 26 (3), 537–557.
Gudmundsson, A., 1992. Formation and growth of normal faults at the divergent plate boundary in Iceland. Terra. Nova 4 (4), 464–471.
Gudmundsson, A., Brynjolfsson, S., Jonsson, M.T., 1993. Structural analysis of a transform fault-rift zone junction in North Iceland. Tectonophysics 220 (1–4), 205–221.
Gudmundsson, A., 1999. Fluid overpressure and stress drop in fault zones. Geophys. Res. Lett. 26 (1), 115–118.
Hjartarson, A., Armannsson, H., 2010. Geothermal research in Greenland. In: Proceedings World Geothermal Congress, pp. 1–8.
Hjartarson, Á., 2011. Víðáttumestu hraun Íslands. Náttúrufræðingurinn 81, 37–49.
Holland, M., Urai, J.L., Martel, S., 2006. The internal structure of fault zones in basaltic sequences. Earth Planet Sci. Lett. 248 (1–2), 301–315.
Homberg, C., Bergerat, F., Angelier, J., Garcia, S., 2010. Fault interaction and stresses along broad oceanic transform zone: Tjörnes Fracture Zone, north Iceland. Tectonics 29 (1).
Hummel, N.V., Waag-Swift, S., Titus, S.J., 2022. Statistical analysis of small faults in rotated blocks of crust near the Húsavík-Flatey transform fault, northern Iceland. J. Geophys. Res. Solid Earth 127 (4), e2021JB022956.
Ikari, M.J., Wilckens, F.K., Saffer, D.M., 2020. Implications of basement rock alteration in the Nankai Trough, Japan for subduction megathrust slip behavior. Tectonophysics 774, 228275.
Kettermann, M., Weismüller, C., von Hagke, C., Reicherter, K., Urai, J.L., 2019. Large near-surface block rotations at normal faults of the Iceland rift: evolution of tectonic caves and dilatancy. Geology 47 (8), 781–785.
Kristmannsdottir, H., Tómasson, J., 1978. Zeolite zones in geothermal areas in Iceland, in natural zeolites: occurrence. In: Sand, L.B., Mumpton, F.A. (Eds.), Properties, Use. Pergamon Press, Elmsford, New York.
Kumar, D., Thiagarajan, S., Rai, S.N., 2011. Deciphering geothermal resources in Deccan Trap region using electrical resistivity tomography technique. J. Geol. Soc. India 78, 541–548.
Liotta, D., Brogi, A., Ruggieri, G., Rimondi, V., Zucchi, M., et al., 2020. Fracture analysis, hydrothermal mineralization and fluid pathways in the Neogene Geitafell central volcano: insights for the Krafla active geothermal system, Iceland. J. Volcanol. Geoth. Res. 391, 106502.
Liotta, D., Brogi, A., Árnadóttir, S., Ágústsson, K., Thorsteinsdóttir, U., 2021. Field evidence of the interplay between rift and transform structures in the Krafla geothermal area, N-Iceland. Geothermics 91, 102039.
Llenos, A.L., Michael, A.J., 2013. Modeling earthquake rate changes in Oklahoma and Arkansas: possible signatures of induced seismicity. Bull. Seismol. Soc. Am. 103 (5), 2850–2861.
Martel, S.J., Langley, J.S., 2006. Propagation of normal faults to the surface in basalt, Koae fault system, Hawaii. J. Struct. Geol. 28 (12), 2123–2143.
Metzger, S., Jónsson, S., Danielsen, G., Hreinsdóttir, S., Jouanne, F., Giardini, D., Villemin, T., 2013. Present kinematics of the Tjörnes fracture zone, North Iceland, from campaign and continuous GPS measurements. Geophys. J. Int. 192 (2), 441–455.
Moore, D.E., Hickman, S., Lockner, D.A., Dobson, P.F., 2001. Hydrothermal minerals and microstructures in the Silangkitang geothermal field along the Great Sumatran fault zone, Sumatra, Indonesia. Geol. Soc. Am. Bull. 113 (9), 1179–1192.
Oelkers, E.H., Gislason, S.R., 2023. Carbon capture and storage: from global cycles to global solutions. Geochemical Perspectives 12 (2), 179–180.
Rempe, M., Smith, S.A., Ferri, F., Mitchell, T.M., Di Toro, G., 2014. Clast-cortex aggregates in experimental and natural calcite-bearing fault zones. J. Struct. Geol. 68, 142–157.
Rhys, D.A., Lewis, P.D., Rowland, J.V., 2020. Structural controls on ore localization in epithermal gold-silver deposits: a mineral systems approach.
Rögnvaldsson, S., Gudmundsson, A., Slunga, R., 1998. Seismotectonic analysis of the Tjörnes fracture zone, an active transform fault in north Iceland. J. Geophys. Res. 103 (30). B12, 117-30, 129.
Saemundsson, K., 1974. Evolution of the axial rifting zone in northern Iceland and the Tjörnes fracture zone. Geol. Soc. Am. Bull. 85, 495–504.
Sæmundsson, K., 1979. Outline of the geology of Iceland. Jokull 29, 7–28.
Saemundsson, K., Karson, J.A., 2006. Stratigraphy and tectonics of the Húsavík-Western Tjörnes area. Techincal report prepared for Alcoa and HRV Engineering, Iceland Geosurvey.

Sibson, R.H., 1994. Crustal stress, faulting and fluid flow. Geological Society. Special Publications, London, pp. 69–84, 78(1).
Sibson, R.H., 1996. Structural permeability of fluid-driven fault-fracture meshes. J. Struct. Geol. 18 (8), 1031–1042.
Sibson, R.H., 2000. Fluid involvement in normal faulting. J. Geodyn. 29 (3–5), 469–499.
Skelton, A., Liljedahl-Claesson, L., Wästeby, N., Andrén, M., Stockmann, G., Sturkell, E., et al., 2019. Hydrochemical changes before and after earthquakes based on long-term measurements of multiple parameters at two sites in northern Iceland—a review. J. Geophys. Res. Solid Earth 124 (3), 2702–2720.
Smeraglia, L., Bettucci, A., Billi, A., Carminati, E., Cavallo, A., et al., 2017. Microstructural evidence for seismic and aseismic slips along clay-bearing, carbonate faults. J. Geophys. Res. Solid Earth 122 (5), 3895–3915.
Smith, S.A., Billi, A., Toro, G.D., Spiess, R., 2011. Principal slip zones in limestone: microstructural characterization and implications for the seismic cycle (Tre Monti Fault, Central Apennines, Italy). Pure Appl. Geophys. 168, 2365–2393.
Stefánsson, R., Gudmundsson, G.B., Halldórsson, P., 2008. Tjörnes fracture zone. New and old seismic evidences for the link between the North Iceland rift zone and the Mid-Atlantic ridge. Tectonophysics 447 (1–4), 117–126.
Sutherland, R., Toy, V.G., Townend, J., Cox, S.C., Eccles, J.D., et al., 2012. Drilling reveals fluid control on architecture and rupture of the Alpine fault, New Zealand. Geology 40 (12), 1143–1146.
Tesei, T., Collettini, C., Barchi, M.R., Carpenter, B.M., Di Stefano, G., 2014. Heterogeneous strength and fault zone complexity of carbonate-bearing thrusts with possible implications for seismicity. Earth Planet Sci. Lett. 408, 307–318.
Tibaldi, A., Bonali, F.L., Einarsson, P., Hjartardóttir, Á.R., Mariotto, F.P., 2016a. Partitioning of holocene kinematics and interaction between the theistareykir fissure swarm and the Húsavik-Flatey Fault, North Iceland. J. Struct. Geol. 83, 134–155.
Tibaldi, A., Bonali, F.L., Pasquaré Mariotto, F.A., 2016b. Interaction between transform faults and rift systems: a combined field and experimental approach. Front. Earth Sci. 4, 33.
Tibaldi, A., Bonali, F.L., Pasquaré Mariotto, F., Corti, N., Russo, E., Einarsson, P., Hjartardóttir, Á.R., 2020. Rifting kinematics produced by magmatic and tectonic stresses in the north volcanic zone of Iceland. Front. Earth Sci. 8, 174.
Vignaroli, G., Viola, G., Diamanti, R., Zuccari, C., Garofalo, P.S., Bonini, S., Selli, L., 2020. Multistage strain localisation and fluid-assisted cataclasis in carbonate rocks during the seismic cycle: insights from the Belluno Thrust (eastern Southern Alps, Italy). J. Struct. Geol. 141, 104216.
Volpe, G., Pozzi, G., Carminati, E., Barchi, M.R., Scuderi, M.M., et al., 2022. Frictional controls on the seismogenic zone: insights from the Apenninic basement, Central Italy. Earth Planet Sci. Lett. 583, 117444.
Volpe, G., Pozzi, G., Locchi, M.E., Tinti, E., Scuderi, M.M., Marone, C., Collettini, C., 2023. Rheological heterogeneities at the roots of the seismogenic zone. Geology 51 (10), 988–992.
Von Hagke, C., Kettermann, M., Bitsch, N., Bücken, D., Weismüller, C., Urai, J.L., 2019. The effect of obliquity of slip in normal faults on distribution of open fractures. Front. Earth Sci. 7, 18.
Vrolijk, P.J., Urai, J.L., Kettermann, M., 2016. Clay smear: review of mechanisms and applications. J. Struct. Geol. 86, 95–152.
Walker, R.J., Holdsworth, R.E., Armitage, P.J., Faulkner, D.R., 2013b. Fault zone permeability structure evolution in basalts. Geology 41 (1), 59–62.
Walker, R.J., Holdsworth, R.E., Imber, J., Ellis, D., 2011. The development of cavities and clastic infills along fault-related fractures in Tertiary basalts on the NE Atlantic margin. J. Struct. Geol. 33 (2), 92–106.
Walker, R.J., Holdsworth, R.E., Imber, J., Ellis, D., 2012. Fault-zone evolution in layered basalt sequences: a case study from the Faroe Islands, NE Atlantic margin. Bulletin 124 (7–8), 1382–1393.
Walker, R.J., Holdsworth, R.E., Imber, J., Faulkner, D.R., Armitage, P.J., 2013a. Fault zone architecture and fluid flow in interlayered basaltic volcaniclastic-crystalline sequences. J. Struct. Geol. 51, 92–104.
Wästeby, N., Skelton, A., Tollefsen, E., Andrén, M., Stockmann, G., Claesson Liljedahl, L., et al., 2014. Hydrochemical monitoring, petrological observation, and geochemical modeling of fault healing after an earthquake. J. Geophys. Res. Solid Earth 119 (7), 5727–5740.
Weisenberger, T., Selbekk, R.S., 2009. Multi-stage zeolite facies mineralization in the Hvalfjördur area, Iceland. Int. J. Earth Sci. 98, 985–999.
Weismüller, C., Urai, J.L., Kettermann, M., von Hagke, C., Reicherter, K., 2019. Structure of massively dilatant faults in Iceland: lessons learned from high-resolution unmanned aerial vehicle data. Solid Earth 10 (5), 1757–1784.
Woodcock, N.H., Mort, K., 2008. Classification of fault breccias and related fault rocks. Geol. Mag. 145 (3), 435–440.
White, J.A., Foxall, W., 2016. Assessing induced seismicity risk at CO2 storage projects: recent progress and remaining challenges. Int. J. Greenh. Gas Control 49, 413–424.
Zhang, L., He, C., Liu, Y., Lin, J., 2017. Frictional properties of the South China Sea oceanic basalt and implications for strength of the Manila subduction seismogenic zone. Mar. Geol. 394, 16–29.
Zhong, Z., Xu, C., Wang, L., Hu, Y., Zhang, F., 2023. Experimental investigation on frictional properties of stressed basalt fractures. J. Rock Mech. Geotech. Eng. 15 (6), 1457–1475.